REVISTA BOLIVIANA DE FÍSICA 20s, 24-26, 2011
ISSN 1562-3823. INDEXADA EN: SCIELO, LATINDEX, PERIÓDICA

Raman Lidar monitors emissions from sugar cane fires in the State of São Paulo: A Pilot-Project integrating Radar, Sodar, Aerosol and Gas observations

G. Held[1], F.J.S. Lopes[2], J.M. Bassan[1], J.T. Nery[3], A.A. Cardoso[4], A.M. Gomes[1], T. Ramires[3], B.R.O. Lima[5], A.G. Allen[4], L.C. da Silva[4], M.L. Souza[4], K.F. de Souza[6], L.R.F. Carvalho[6], R.C. Urban[7], E. Landulfo[2], A.M. de Decco[1], M.L.A.A. Campos[7], M.E.Q. Nassur[7], R.F.P. Nogueira[4]

[1] Instituto de Pesquisas Meteorológicos, UNESP, Bauru, S.P., Brazil
Tel: +55 14 3103-6030, Fax: +55 14 3203-3649, E-nail: gerhard@ipmet.unesp.br
[2] Centro de Lasers e Aplicações, IPEN/CNEN, São Paulo, S.P., Brazil
[3] Campus Experimental de Ourinhos, UNESP, Ourinhos, S.P., Btazil
[4] Instituto de Química, UNESP, Araraquara, S.P., Brazil
[5] Instituto de Geociências, Unicamp, Campinas, S.P., Brazil
[6] Instituto de Química, USP, São Paulo, S.P., Brazil
[7] Departemento de Química, USP, Riberão Preto, S.P., Brazil

SUMMARY

Ourinhos is situated in one of the major sugar cane producing regions in the State of São Paulo, where the manual harvesting is generally preceded by burning the foliage, resulting in large quantities of aerosols being emitted into the atmosphere. A one-month pilot study was executed during August 2010, to characterize the effects of those emissions on the atmosphere, considering the local circulation and the consequences for the region. The plumes were tracked by IPMet´s two S-band Doppler radars, also deploying a large range of meteorological, physical and chemistry instrumentation: a mobile Lidar with Raman channel to observe elevated layers and the type of aerosols, a medium-sized Sodar, as well as 6 Automatic Weather Stations spread through town. Various gases and particulates were also sampled, providing the atmospheric chemistry data base and thus documenting the impact on the region.

This paper highlights a case study on 26 August, when a plume was tracked by TITAN Radar Software from the start of the fire, moving southwards at 14-17 km.h^{-1} with the winds at about 3,5 km above ground level, until it reached Ourinhos 2h15min later, where it was observed by the Raman Lidar and also detected by the aerosol and gas samplers. The high aerosol load of the atmosphere was confirmed by hourly mean values of AOD varying between 0,265 and 0,288 until 07:00 LT, after which they increased to 0,433 by 09:00 LT, as well as hourly mean backscatter profiles. Hourly values of the Lidar Ratio identified the aerosols as biomass burning products, also confirmed through the analysis of gas and aerosol samples simultaneously collected at the Lidar site.

Key words: Raman Lidar, biomass fire plumes, Doppler Radars, Sodar, Aerosol & Gas Sampling

INTRODUCTION

Ourinhos is situated in one of the major sugar cane producing regions in the State of São Paulo, where the sugar cane is harvested from April until November. Sectors of the plantations are generally burnt prior to manual harvesting. This practice results in large quantities of aerosols being emitted into the atmosphere, not only negatively affecting local towns, but also regions much further away (Held *et al.*, 2011). A one-month pilot study was executed during August 2010, to characterize the effects of those emissions on the atmosphere, considering the local circulation and the consequences for the region. In the absence of rain during the dry winter season, the plumes were tracked by IPMet´s two S-band Doppler radars, also deploying meteorological, physical and chemistry instrumentation: a mobile Lidar with Raman channel to observe elevated layers and the type of aerosols, a medium-sized Sodar, as well as 6 Automatic Weather Stations spread through town. Gases and particulates were also sampled, providing the atmospheric chemistry data base and thus documenting the impact on the region.

METHOD AND RESULTS

The region of Ourinhos was chosen, because the local Campus of UNESP (Universidade Estadual Paulista) maintains a network of 6 Automatic Weather Stations (plus one from INMET, the National Meteorological Institute), and it falls within the 100-120 km range of IPMet´s radar in Bauru (Figure 1), facilitating the tracking and quantitative analysis of such plumes in real time.

Figure 1. IPMet's radars with their quantitative range.

Instrumentation

The Lidar, Sodar, radiosonde and air quality monitoring equipment (particulate samplers and active gas monitors) were all installed at the UNESP Campus in Ourinhos on the north-western outskirts of town (448 m above mean sea level - amsl), as well as the Automatic Weather Station (AWS) of INMET.

The mobile bi-axial Raman Lidar system uses a commercial pulsed Nd:YAG laser, operating at a wavelength of 532 nm, with a pulse energy of 130 mJ at 20 Hz PRF. The pulse width is 25 ns, yielding a spatial resolution of 7,5 m. A detailed description of the system is found in Landulfo *et al.* (2010). The system allows the determination of the optical properties of the atmosphere, like Backscatter Coefficient, Coefficient of Extinction (quantification of aerosol loading of the atmosphere) and the Lidar Ratio (indication of types of aerosols).

The vertical range of the Sodar was set at 800 m above ground level (AGL), with a vertical resolution of 10 m and sampling intervals of 60 min averaged every 30 min on a sliding scale. The products generated are horizontal wind speed & direction, vertical wind velocity, as well as by inference the estimated height of the thermal inversion.

IPMet's radars cover the central and western State of São Paulo (Figure 1). Both have a 2° beam width and a quantitative range of 240 km, generating a volume-scan every 7,5 minutes, with a resolution of 250 m radially and 1° in azimuth, recording reflectivities and radial velocities at 16 elevations. However, in order to register and track the *queimadas*, a special scanning cycle was introduced to provide a better vertical resolution up to the anticipated detectable top of the plumes: 10,0º; 8,0º; 6,5º; 5,0º; 4,0º; 3,2º; 2,4º; 1,6º; 0,8º; 0,3º, with each "sweep" (PPI) having 360 rays with 957 range bins each. Two different systems of Software were deployed, *viz.* IRIS (*Interactive Radar Information System*) Analysis, to first generate CAPPIs (*Constant Alitude PPIs*) at 1,5 and 2,0 km amsl in order to identify all *queimadas* within the 240 km range of the radars. Once a *queimada* was identified to pass over the monitoring site, it was tracked by the TITAN (Thunderstorm Identification, Tracking, Analysis and Nowcasting; Dixon and Wiener, 1993) Software to determine its intensity (based on radar reflectivity in dBZ), horizontal and vertical dimensions, and the velocity of approach. The thresholds used for tracking were 10 dBZ with a minimum volume of 2 km^3. It should be noted, that TITAN uses Universal Time (Local Time LT = UT-3h).

Since it is extremely important for the population in the Region to characterize the air quality, some gases (NO_2, SO_2, O_3, Aldehydes) monitored and soluble aerosols sampled in different size fractions, including elementary carbon, during different periods of the day (10:00-16:00 and 20:00-06:00 LT), and also Polycyclic Aromatic Hydrocarbons (HPA). Ion chromatographic analysis would allow the identification of possible sources, especially biomass burning products, like Potassium (K^+) and water-soluble organic carbon (WSOC).

Case Study of 25-26 August 2010

Based on a synoptic analysis for the Ourinhos Region, the month of August can be divided into two distinct periods, *viz*., 01-15 August, when 3 cold fronts crossed the State, causing light rain and very low temperatures especially at the beginning of the month, while during the second half the weather was dominated by a high pressure system, resulting in the temperatures to rise, but with low humidity, favoring the accumulation of pollutants in the regional air. The case study from 25 to 26 August 2010 was characterized by exactly such conditions.

The first echo of a smoke plume was detected by the Bauru radar on 26 August 2010 at 00:08 LT, about 35 km north-north-east of Ourinhos and ca 85 km south-west of the radar, rapidly gaining in area and intensity (≤40 dBZ near its origin). By 00:22 LT, TITAN could already identify its centroid and tracked it until 02:45 LT, when the plume had already spread over Ourinhos. As the plume moved southwards with the northerly winds, the aerosols spread out (dispersed) and the reflectivity dropped gradually until 02:45 LT, but it could still be detected by the radar until 03:46 LT, >20 km south of Ourinhos, using a reflectivity threshold of -6 dBZ.

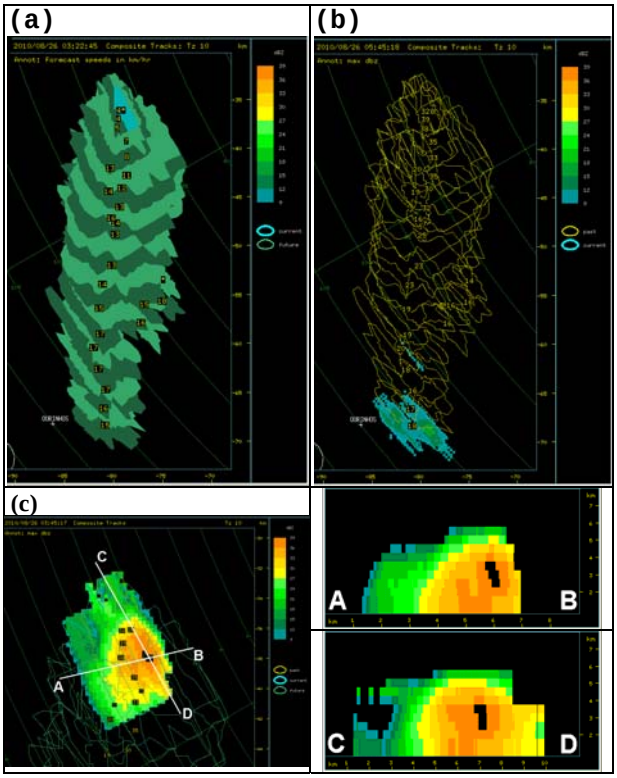

Figure 2: Tracks generated by TITAN on 26 August 2010. The envelopes (10 dBZ reflectivity) show the position of the *queimada* in intervals of 7,5 min (blue = actual time; green = future; yellow = past).
(a) First TITAN centroid of the *queimada* (fire) at 03:22UT (00:22LT; annotation: propagation velocity in km.h^{-1});
(b) The *queimada* reached the Ourinhos area at 05:45UT (02:45LT; annotation: max reflectivity in dBZ);
(c) Max-CAPPI and cross-sections, showing the horizontal and vertical extent along the base lines at 03:45UT.

Although during the night from 25 to 26 August, there were several other *queimadas* active and contributing to the overall aerosol load in the region, this study only concentrates on the history of the above plume, as illustrated by the TITAN-generated images in Figure 2.

Furthermore, it can be deduced from Figure 2a, that while the plume was at low heights at the beginning, it moved very slowly (3-4 km.h^{-1}) since the wind speed in the first few hundred meters was very low (≤5 m.s^{-1}), as observed by the Sodar. It also showed a shift of the wind direction from

easterly to northerly winds >300 m AGL. These northerly winds were above the nocturnal surface inversion and are confirmed by the "Skew T x Log P" profiles of the Meso-Eta Model in the layer 900-800 hPa (650–1650 m AGL). The vertical velocity w indicated that downward mixing of the pollutants (aerosols), trapped above the inversion, only commenced at around 09:00 - 09:30 LT, since from 00-06 LT and from 06-09:00 LT the atmosphere was extremely stable below 300 m AGL (w = ±0 m.s^{-1}).

The Lidar was operating continuously from 25/08/2010 to 27/08/2010, also recording the Raman Channel during the night. Considering the radar images in Figure 2, the *queimada* arrived over the municipal area of Ourinhos between 02:30 and 02:45 LT. Figure 3 visualizes the Lidar observation between 00:00 and 06:00 LT up to a height of 3 km AGL. The arrival of the *queimada* aloft is marked with an arrow. Furthermore, a distinct cut-off at ca 2,6 km AGL is visible, which coincides with the top of the Planetary Boundary Layer, above which a very dry and relative warm and clean air was advected from the west above ca 730 hPa, creating an elevated inversion which blocked further upward mixing. The lowest layer ≤250 m AGL appears clean, being trapped within the surface inversion, which inhibits downward mixing, also confirmed by the Sodar measurements, indicating a very stable layer. Above it, during the first hours of the day, regional remnants of aerosols are observed, until the plume arrived at 02:40 LT between 350 and 600 m AGL, being transported by northerly winds.

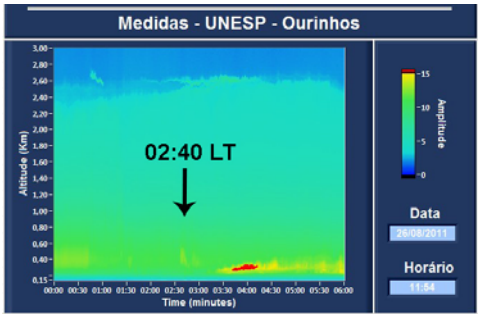

Figure 3. LIDAR signal (arbitrary units) visualized from 00:00-06:00 LT up to 3 km AGL.

A quantitative analysis of the Lidar observations was performed by first integrating the data from the Raman Channel (non-elastic signal at 607 nm) into hourly means until 09:00LT to obtain the Aerosol Optical Depth (AOD). The results confirmed a high aerosol load of the atmosphere, with hourly mean values of AOD varying between 0,265 and 0,288 until 07:00LT, thereafter increasing to 0,433 by 09:00 LT.

Backscatter Profiles at 532 nm were generated for every hourly integrated period, showing an aerosol load up to about 2,6 km AGL. The first Backscatter profiles (00:00-02:59 LT) represent the regional pollution load, while from 03:00 LT onwards, a specific plume (as identified by TITAN, Figure 2) arrived at Ourinhos above the temperature inversion. Thereafter, the Backscatter Signal peak gradually increased from 0,003 to 0,004 km^{-1}.sr^{-1} at 03:40-04:20 LT, with a further increase to 0,0056 km^{-1}.sr^{-1} by 11:00 LT, after which the peak of the Backscatter Signal is decreasing due to turbulent mixing of the atmosphere.

Hourly means of the Lidar Ratio show an increase during the period 02:00-02:59 LT, confirming the arrival of the *queimada* from the north, while an almost 20% increase to 72 sr after 07:00 LT is probably due to downward mixing of the nocturnal *queimadas*, also confirmed by an increase of AOD values from the Raman signal. According to Catrall *et al.* (2005), aerosols originating from biomass burning have LR values between 59 and 70 sr. Omar *et al.* (2009) also suggest LR values of around 70 sr for biomass aerosols. Following these suggested values, the LR calculated for the observations on 26 August 2010 are most likely due to aerosols generated during biomass fires in the region.

CONCLUSIONS

In conclusion, it can be confirmed, that the smoke plume emitted by a sugar cane fire, observed by IPMet´s Bauru radar and tracked with the TITAN Software did reach the municipal area of Ourinhos during the early hours of the morning of 26 August 2010, and was also registered by the Lidar in a layer above 350 m AGL, but was initially prevented from mixing downwards by the very stable atmospheric conditions, as implied by low aerosol concentrations collected during the nocturnal period 22:00 – 06:00 LT. However, the chemical analyses (10:00 – 16:00 LT), as well as the Lidar parameters, pointed at daytime downward mixing of the suspended aerosols, as soon as the stable Boundary Layer conditions were eroded by increasing daytime temperatures. This, in turn, would directly result in a negative impact on the health and well-being of the population in that region. Relatively high background concentrations of aerosols observed at the monitoring site indicate an accumulation of pollutants during prolonged periods of stable atmospheric conditions, being responsible for respiratory problems of the population due to the very fine particulate matter in suspension.

ACKNOWLEDGMENTS

FUNDUNESP is thanked for support to conduct the collection of meteorological and Lidar data during this Pilot Campaign (Processo 00598/10-DFP) and to present the paper. The chemical sampling was done by participants of FAPESP Project "Effects of emissions on current and future rainfall patterns in Southeast Brazil" (Processo No. 2008/58073-5).

REFERENCES

Cattrall C, Reagan J, Thome K and Dubovik O, 2005. Varia-bility of aerosol and spectral lidar and backscatter and extinction ratios of key aerosol types derived from selected Aerosol Robotic Network locations, *Journal of Geophysical Research*, **110**, D10S11.

Dixon M and Wiener G, 1993. TITAN: Thunderstorm Identi-fication, Tracking, Analysis & Nowcasting - A radar-based methodology, *J. Atmos. Oceanic Technol*., **10**, 785-797.

Held G, Landulfo E, Lopes FS, Arteta J, Marecal V and Bassan JM, 2011. Emissions from sugar cane fires in the central & western State of São Paulo and aerosol layers over Metropolitan São Paulo observed by IPEN´s lidar: Is there a connection? *Opt.Pura. Apl.*, **44** (1), 83-91.

Landulfo E, Jorge MP, Held G, Guardani R, Steffens J, Pinto SdAF, Andre IR, Garcia A G, Lopes FJS, Mariano GL, da Costa RF and Rodrigues PF, 2010. Lidar observation campaign of sugar cane fires and industrial emissions in the State of São Paulo, Brazil. *SPIE Digital Library, Proc. SPIE,* Vol. **7832**, 783201 (2010), 8pp; doi: 10.1117/12.866078.

Omar AH, Winker DM, Kittaka C, Vaughan MA, Liu Z, Hu Y, Trepte CR, Rogers RR, Ferrare RA, Lee KP, Kuehn RE and Hostetler CA, 2009. The CALIPSO Automated Aerosol Classification and Lidar Ratio Selection Algorithm, *Journal of Atmospheric and Oceanic Technology*, **26**, 1994-2014.

REVISTA BOLIVIANA DE FÍSICA 20s, 27-29, 2011
ISSN 1562-3823. INDEXADA EN: SCIELO, LATINDEX, PERIÓDICA

Comparison of AOD measurements and forecasts of Saharan dust events at Camagüey, Cuba.

Juan Carlos Antuña[(1)], Victoria Cachorro[(2)], René Estevan[(1)], Ángel de Frutos[(2)], Boris Barja[(1)], Yasmine Benouna[(2)], Benjamín Torres[(2)], David Fuertes[(2)], Ramiro González[(2)],Carlos Toledano[(2)], George Kallos[(3)] and Spyrou Christos[(3)]

[(1)]Grupo de Óptica Atmosférica de Camagüey, Centro Meteorológico de Camagüey, Camagüey, Cuba
[(2)]Grupo de Óptica Atmosférica, Universidad de Valladolid, España
[(3)]Department of Applied Physics, University of Athens, Greece

E-mail: anadelia@caonao.cu

SUMMARY

The SKIRON model AOD forecasts for Saharan dust clouds arriving to Camagüey, Cuba, during July 2009 were evaluated. For such a goal AOD measurements from a surface sunphotometer were used. Additional information from MODIS was also available for the comparison. The results demonstrate the capabilities for developing an alert and tracking system for Saharan dust events across the Atlantic.

Key words: Saharan dust, aerosols, AOD, SKIRON model

INTRODUCTION

Recent studies using state of the art satellite information showed that every year 240 ± 80 Tg of dust are transported from Africa in the latitude band 20°S – 30°N. From that amount 50 ± 15 Tg are deposited in the Amazon basin and 50 ± 25 Tg arrive to the Caribbean (Kaufman et al., 2005). Those enormous amounts of aerosols have an important impact in human activities

The GOAC team, in cooperation with scientists from several institutions is developing a service for alert-tracking the Saharan dust transported over the Atlantic to the Wider Caribbean. The core idea of the service is to provide, to each one of the countries of the Wider Caribbean local notices of the future arrival of Saharan dust to his area combined with updates of the current position of the dust air masses. It will combine existing numerical modelling of the Saharan dust transport with satellite and surface observations. Those sources of information are the SKIRON model AOD forecasts, the derived AOD from MODIS (both from Terra and Aqua) and the derived sun photometer AOD. The purpose of the present comparison is to have a preliminary estimation of the magnitudes of the differences between the AOD sun-photometer measurements at Camagüey and the coincident AOD forecasted by SKIRON in the presence of several Saharan dust events.

DATASETS

The sun photometer CIMEL CE-318 installed at the Camagüey (21.42º N, 77.84º W, 128 meters over sea level) is part of the Iberian Network for Aerosol Measurements (RIMA) which is federated into the Aerosol Robotic Network (AERONET). It was installed as result of a cooperation agreement for joint aerosol research between the University of Valladolid (UVA), Spain, and the Cuban Meteorological Institute (INSMET). The research are conducted by the Grupo de Óptica Atmosférica (GOA-UVA) and the Grupo de Óptica Atmosférica de Camagüey (GOAC-INSMET), formerly the Camagüey Lidar Station. The sun-photometer was operative from October 7th 2008. After the post calibration of the CIMEL # 353 and the reprocessing of the dataset the produced AOD by AERONET Version 2.0 showed very little changes with respect to the Version 1.5.

From the total of 746 instantaneous AOD measurements that passed the quality control and were processed in the Version 1.5 for the entire month of July 2009, only 11 did not passed the quality control required for version 2.0, representing only the 1.5% of the observations reported before. The rest of the AOD values (98.5%) did not changed in the Version 2.0 with respect to the Version 1.5. Table 1 lists the day's data has been discarded in Version 2.0 and its effects respect to Version 1.5.

Table No. 1: Daily distribution and observed effect on the AOD values of discarded observations per day in Version 2.0 with respect to Version 1.5. Period July 1st to 31st 2009.

Day	# Obs.	Observed effect on Version 2.0 AOD
2	1	Daily Mean AOD decrease in 0.0089
3	5	No AOD values for that day
10	2	No AOD values for that day
11	3	Daily Mean AOD decrease in 0.0726

Saharan dust events were measured by first time with the sun-photometer installed at Camagüey, Cuba, in July 2009.

Those had been already studied [*Estevan et al.*, 2011]. We selected that period of time because of the presence of several events in the course of the month

The SKIROM model has been operational for more than 10 years. Recently a new upgraded version has been released (Kallos et al., 2009). For the present comparison we have used the SKIRON griddled (0.1° x 0.1°) daily hourly forecasts of AOD at 500 nm, from July 1st to 31st, 2009. For the purposes of the comparison we selected the AOD values in the area of 0.5º x 0.5º around the Camagüey sunphotometer site. That grid box covers and area of 2874.5 km^2. (ΔX = 51.7 km and ΔY = 55.6 km).

RESULTS AND DISCUSION

Camagüey AOD measurements

The Camagüey AOD dataset (Version 2.0) for July 2009 consists of 735 instantaneous measurements. The data was processed attending to three different criteria:

1. Hourly mean AOD **(H-AODCMG):** For each hour, each day the mean AOD value was calculated, resulting in 239 H-**AODCMG** values.
2. Daily mean AOD **(D-AODCMG):** For each day the mean AOD value was calculated, resulting 29 **D-AODCMG** values.
3. Daily maximum **AOD (DMx-AODCMG):** For each day the maximum AOD value was calculated, resulting in 29 AOD{max} values. Also the time of the occurrence of the **DMx-AODCMG** values were registered.

The figure 1 depicts on the top panel the set of instantaneous measurements for the whole period of study (black dots). In the middle panel appear the hourly mean values. In the bottom daily means and maximum are plotted.

SKIRON forecasts dataset:

Different magnitudes of the AOD were calculated:

1. Hourly mean AOD (**H-AODSK**): Average of the AOD over the selected grid box for each one of the 24 hours each day. (744 values)
2. Hourly maximum AOD (**HMx-AODSK**): Maximum value of the AOD over the selected grid box for each one of the 24 hours each day. (744 values)
3. Daily means AOD (**D-AODSK**): Average of the AOD over the selected grid box and over the 24 hours each day. (31 values)
4. Daily coincident maximum AOD (**DMx-AODSK**): Maximum value of the forecasted AOD over the selected grid box for each one of the 24 hours each day for the same hour the daily maximum AOD at Camagüey was registered. (31 VALUES)

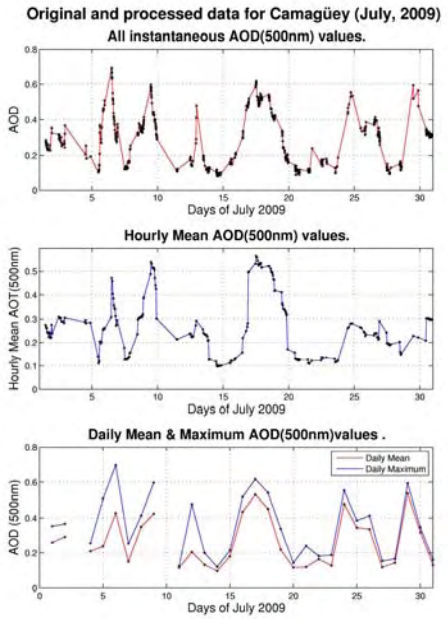

Figure 1. Results of the processing of AOD sun-photometer measurements at Camagüey.

Comparison

The figure 2 shows the differences between the hourly mean AOD measured at Camagüey (**H-AODCMG**) by sunphotometer and the hourly mean AOD (**H-AODSK**) forecasted by SKIRON. The last values were selected considering the values nearest in time to the hour the sunphotometer measurement was conducted (239 pair of values). Those differences are depicted in blue. For illustrative purposes the values of **H-AODCMG** are also plotted (green).

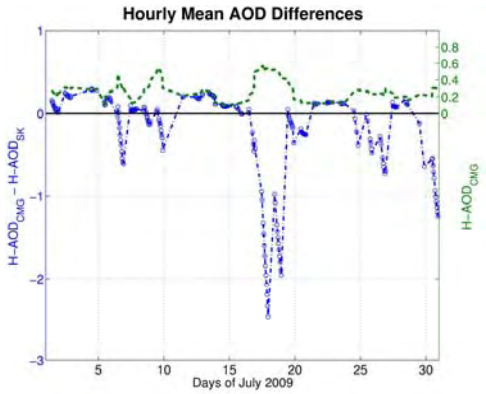

Figure 2: Hourly mean AOD differences.

The higher differences in figure 2 are associated with the maximum values of the AOD registered by sunphotometer at Camagüey caused by Saharan aerosols, all then negatives. This is a consequence of the Saharan aerosols AOD values forecasted by SKIRON being higher than the measured ones. In the cases of the lower AOD values measured, in absence of Saharan aerosols, the differences are mainly positive, revealing that in that case the AOD values forecasted by SKIRON being lower than the measured ones. In several

cases the forecasted AOD values are very little, almost zero, producing differences of the same magnitude than the measured AOD. This feature is produced by the fact that SKIRON do not takes into account the background aerosols (and its corresponding AOD) produced by local sources.

Figure 3 shows the difference between the daily mean AOD measured (**D-AODCMG**) and the daily mean AOD forecasted by SKIRON (**D-AODSK**). In general there is a decrease of the differences, with less negative cases, but the main features discussed in figure 2 remain.

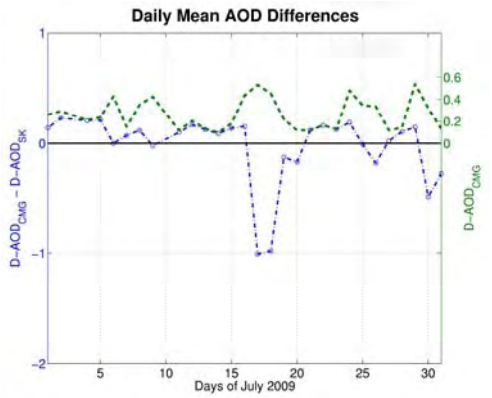

Figure 3: Daily mean AOD differences.

Figure 4 shows the difference between the measured daily maximum AOD (**DMx-AODCMG**) and the forecasted daily maximum AOD (**HMx-AODSK**). It resembles almost the same behavior that the hourly mean AOD differences in figure 2.

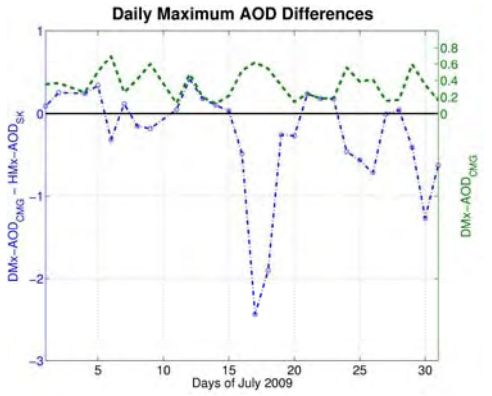

Figure 4: Daily maximum AOD differences.

In figure 5 is shown the plot of the differences between the daily maximum AOD measured (**DMx-AODCMG**) and the forecasted daily maximum AOD at the same hour the maximum AOD was registered (**DMx-AODSK**). The differences are in the same order of magnitude than the **DMx-AODCMG**, due to the fact that the **DMx-AODSK** has very low values.

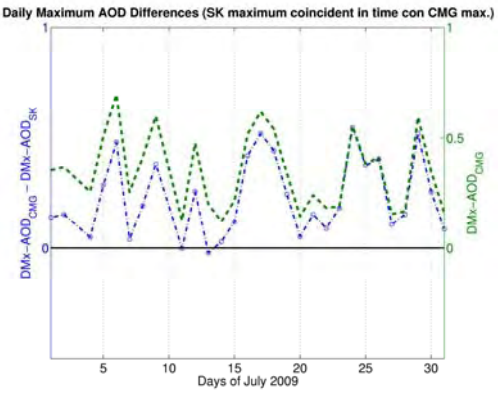

Figure 5: Daily maximum AOD differences. Forecasted AOD maximum determined at the same hour than the maximum measured AOD.

CONCLUSIONS

From the former results several preliminary conclusions have been obtained. The daily average values of the sunphotometer measured and modeled forecasted AOD show the better agreement, but still notable differences are present. The lack of background aerosols AOD in the forecast produces additional differences in the absence of Saharan dust. In the case of the long range transport of Saharan aerosols the forecasted AOD values are higher than the measured ones.

Current work is in progress to improve the comparisons and to conduct also comparisons with coincident MODIS AOD observations.

REFERENCES

Estevan, R., J. C. Antuña, B. Barja, V. E. Cachorro, Á. M. de Frutos, A. Berjón, C. Toledano, B. Torres, R. Rodrígo, T. A. Hernández y C. E. Hernández, 2011: Preliminary results of aerosols measurements with sun photometer at Camagüey, Cuba. Opt. Pura Apl., 44 (1), 99-106.

Kallos, G. C. Spyrou, M. Astitha, C. Mitsakou, S. Solomos, J. Kushta, I. Pytharoulis, P. Katsafados, E. Mavromatidis, N. Papantoniou and G. Vlastou, 2009: Ten-year operational dust forecasting - Recent model development and future plans. IOP Conf. Series: Earth and Environmental Science, 7, 012012, doi:10.1088/1755-1307/7/1/012012.

Kaufman, Y. J., Koren, I., Remer, L. A., Tanr´e, D., Ginoux, P., and Fan, S., 2005: Dust transport and deposition observed from the Terra-Moderate Resolution Imaging Spectroradiometer (MODIS) spacecraft over the Atlantic Ocean, J. Geophys. Res., 110, D10S12, doi:10.1029/2003JD004436.

REVISTA BOLIVIANA DE FÍSICA 20s, 30-32, 2011
ISSN 1562-3823. INDEXADA EN: SCIELO, LATINDEX, PERIÓDICA

Remote control and telescope auto-alignment system for multiangle lidar under development at CEILAP, Argentina

Juan V. Pallotta, Pablo Ristori, Lidia Otero, Francisco Gonzalez, Juan Carlos Dworniczak, Raul D'Elia, Ezequiel Pawelko, Eduardo Quel.
CEILAP (CITEDEF-CONICET), UMI-IFAECI-CNRS 3351
Juan B. de La Salle 4397, B1603ALO Villa Martelli – Buenos Aires, Argentina.
E-mail: jpallotta@citedef.gob.ar
Alberto Etchegoyen
ITeDA (CNEA – CONICET - UNSAM)
Av. Gral. Paz 1499 - 1650 San Martín – Buenos Aires, Argentina.

SUMMARY

At CEILAP (CITEDEF-CONICET), a multiangle Raman lidar is under development to monitor aerosol extinction in the frame of the CTA (Cherenkov Telescope Array) Project. This is an initiative to build the next generation of ground-based instruments to collect very high energy gamma-ray radiation. It will serve as an open observatory for a wide astrophysics community and will explore the Universe in depth in Very High Energy (> 10 GeV) gamma-rays. The atmospheric conditions are is a major interest for CTA, and this instrument plays a major role measuring the atmospheric optical depth.
The reception system is made by six 40 cm in diameter Newtonian telescopes, totally exposed to the hard environmental condition during the shifts. These working conditions could produce misalignments between laser and telescopes, losing the required overlap. To avoid that, a telescope controlled by a self-alignment system is under development to solve this problem. This is performed by PC software running from the acquisition module which is connected via ethernet to a microcontroller. This paper, describes the self-alignment method and hardware work in progress.

Key words: multiangle lidar, Raman, CTA observatory, aerosols.

INTRODUCTION

The Cherenkov Telescope Array Consortium (CTA) contemplates the design, construction and the operation of two observatories for the detection of gamma-ray produced by extraterrestrial sources at energies range between 10^{10} eV to 10^{14} eV. These observatories will be deployed at each hemisphere for full sky-map coverage. Each Observatory will consist of a telescope array sensitive to the atmospheric generated Cherenkov radiation that will improve the performance of the actual detectors. The objectives proposed for CTA will be attained using an array of multiple telescopes distributed over a surface of 1 km^2, located at sites with excellent optical and atmospheric conditions at a height of 2000 to 3500 mts above the sea level. The comprehension of the atmospheric conditions during the measurements is extremely important for the CTA Observatory. In fact, the atmosphere acts as the first detector at which the air showers are developed. The array of detectors observe the gamma ray induced cascades by measuring the Cherenkov light produced by their charged particles moving above the speed of light of the surrounding atmosphere. The emitted light is attenuated from the source to the telescope due to molecular, aerosol and cloud extinction. Lidars play a leading role in monitoring of sky conditions, by both detecting the overall cloud coverage and measuring the atmospheric opacity due to aerosol and clouds over the Observatory. The location of this astronomical facility will be selected after a careful study of the preselected zones, regarding the latitude, altitude, the atmospheric conditions, and the available local infrastructure. At the Southern hemisphere, Argentina is one of the candidate countries for the installation of the CTA Observatory. The places proposed are "El Leoncito", located in San Juan state and "El CASLEO", in Salta.

LIDAR HARDWARE

LIDAR telescope is planned to be mounted on a steerable frame, and moved using two DC servomotors, reading its position by two relative encoders.

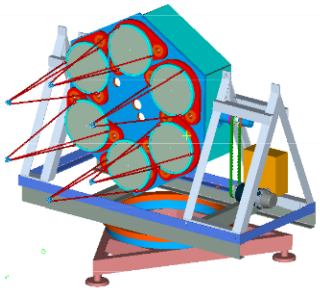

Figure 1. A preliminary sketch of the multiangle lidar under construction.

Movements are handled by a microcontroller that communicates with the lidar PC through an ethernet connection. Each LIDAR is equipped with a Nd:Yag laser, that generates laser pulses at 355, 532 and 1064 nm at a repetition rate of 50 Hz and a pulse energy of ~20 mJ @ 355 nm. The backscattered light is collected by six Newtonian telescopes with 40 cm diameter, 1 m focal length. A

multiwavelength spectrometer separates the backscattered wavelengths and concentrates the light into several Hamamatsu H6780 photomultipliers. A Licel TR20-160 module is used to digitalize and store the lidar profiles

This lidar has special requirements:

- It has to be able to be operated remotely. The lidar operator may not have an a priori knowledge on lidar techniques.
- Telescopes, mechanics and electronics, will be exposed during nighttime to extreme environmental conditions (wind burst, temperature span, etc.), which could produce lidar misalignments

These are the main reasons that encourage the development of a fully automatic alignment system is to keep the telescopes aligned during the acquisition period.

LIDAR COMUNICATIONS

The lidar system under development has two operational modes: *local mode* and *remote mode*. *Local mode* was developed for maintenance procedures. The presence of a lidar technician is required on site to perform hardware improvements and specific tests. *Remote mode* was programmed to perform shift operations. In this case the lidar will be remotely operated and monitored from the control center. The lidar computer was designed to communicate with control center server wirelessly via a WiFi link, creating a local lidar network under the TCP/IP protocol.

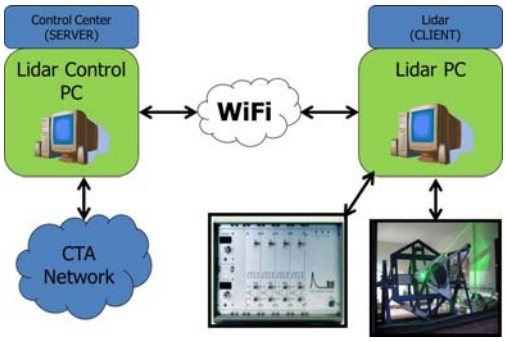

Figure 2. A general schematic layout of the lidar communication system. If remote mode is set, the shifter can monitor and control all the operations.

At the link endpoints, several processes communicate with each other to send/receive control and monitoring messages.

LIDAR SOFTWARE

A more detailed view of the process at each lidar PC can be seen on Figure 3. Each computer works under Linux operating system and all the software was developed in C/C++. A socket-based IPC (Inter Process Communication) was programed to communicate the local with the remote process. To increase their efficiency, each process is totally independent, and communicates to the other via control messages.

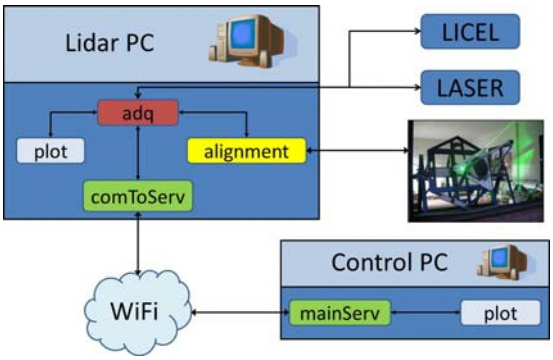

Figure 3. A general diagram about connections in both sides of the lidar system.

A brief description of each process at both sides of the link is described below:

Lidar PC side (client):
adq: Is the main process at the client (lidar) side. It controls the acquisition timing, it communicates with the laser, it triggers the Licel, it sends the acquired new file to the *plot* process, and, if necessary, to the *alignment* process.
plot: Waits messages from the *adq* process, conformed mainly by the new acquired file path and shows it on the display.
comToServ: This process handle all the messages from/to the client/server side.
alignment: This process receive the path to the acquired file from *adq* and process this signal to obtain the alignment parameters to determine the telescope position.
Control PC side (server):
mainServ: Handle the communication between the shifter and the client PC.
plot: Shows the lidar signal from the last saved file.

MICROCONTROLLER-CONTROLLED TELESCOPES

The tilt angle of the telescopes is driven by a set of stepper motors, handled by a RCM2200 Rabbit System microcontroller. This is Z80 family-based high-performance 8 bit microcontroller. It has a built-in Ethernet interface with an integrated TCP/IP stack, making it a good choice for interconnectivity. This interface is used to link the microcontroller with the lidar PC. The instruction set is based on the original Z80 microprocessor, with some additional instructions.
The aims of the Rabbit microcontroller algorithm is to decode the Ethernet information received from the lidar PC *alignment* process, and to handle the signals to correct the stepper motor drivers. The message from the lidar PC to the Rabbit microcontroller has 3 parameters: motor to be controlled, direction and number of steps. Therefore, the firmware of the Rabbit microcontroller is a "dummy terminal" that only receives message and drives the motor. After that, it sends an acknowledge message back to the *alignment* process.

ALIGNMENT ALGORITHM

The alignment algorithm is a cooperative procedure between the *adq* and the *alignment* processes, both running on the lidar PC, and a firmware recorded in the Rabbit microcontroller.
When the alignment mode is set at the *adq* process, each path of the acquired file is sent to *alignment*. Moreover, after

saving a new file at the lidar PC, this file is transferred to the control PC for a backup. A summarized procedure flowchart can be seen on Figure 5.

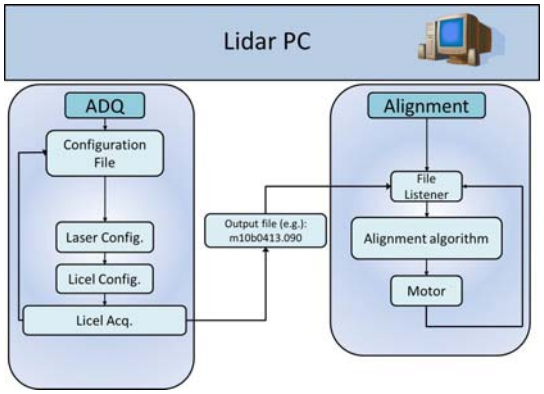

Figure 4. Communication Diagram between the *acquisition* and the *alignment* processes. Both are fully independent, and they communicate via the IPC socket, implemented under C/C++.

The aim of the alignment algorithm is to quantify the alignment state of the recently acquired file and to save it with its tilt position in a table. After that, *alignment* tilts the telescope to a new position and sends an acknowledge message to *acq*, to trigger new acquisition.
The alignment state quantification is obtained by accumulating the lidar signal over certain range, as it seen on the next figure:

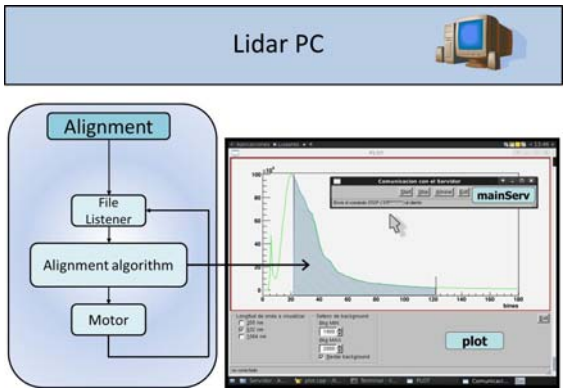

Figure 5.

After finishing the scanning process, the microcontroller sets the telescope position to the one at wich the maximum value was attained. This procedure tends to increase the lidar signal in a wide dynamic range.

FIRST RESULTS

This algorithm was successfully tested, comparing the vertical lidar signals obtained with the ones obtained by the MWRL lidar at CEILAP (CITEDEF-CONICET). The test was done for a vertical fixed position, as can be seen on Figure 4.
The CEILAP's telescope was manually aligned to provide the reference signal. The tested telescope was left intentionally misaligned to test the optimization algorithm.

Figure 4. Picture of the setup of lidar intercomparison.

After turning on the alignment mode, the algorithm exhibited good results, approaching the telescope's signal under test to the reference lidar signal. The next figure shows the lidar signals after the alignment process.

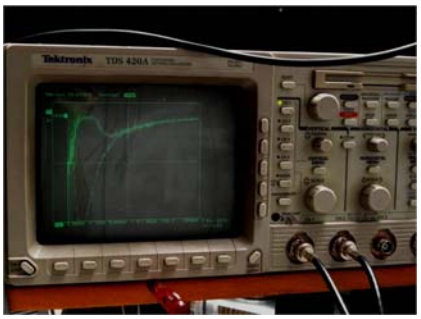

Figure 5. Picture of the lidar signals intercomparison after alignment algorithm success.

The differences seen on the last figure are due to the different distance to the laser source of the systems. Figure 5 shows the long range agreement of the signals.

CONCLUSIONS

The system is ready to be tested in a slant path fixed angle. The lidar is actually being installed inside a container to perform this new test. A new enhanced version of the controlled telescope actuators is under construction. First measurements indicate that it will be possible to achieve the expected auto-optimizations goals during the scanning procedure. The new software for a multiangle lidar prototype is fully operational.

ACKNOWLEDGMENTS

Authors wish to thank JICA, ANCyPT, the CITEFA main workshop's technicians and José Luis Luque from the CEILAP workshop for their support on this development.

REFERENCES

Otero, L. A. *et al.* (2004). First Aerosol Measurements with a Multiwavelength LIDAR System at Buenos Aires, Argentina Proceedings of the Conference of the ILRC2004.

http://www.digi.com/
http://www.cta-observatory.com/,
http://astrum.frm.utn.edu.ar/CTA-Argentina/
Licel programing examples and documentation: http://www.licel.com/soft_tcp.html

REVISTA BOLIVIANA DE FÍSICA 20s, 33-35, 2011
ISSN 1562-3823. INDEXADA EN: SCIELO, LATINDEX, PERIÓDICA

Rayleigh lidar temperature profiles between 15 - 60 km during OZITOS campaign in Río Gallegos (51° 55'S, 69° 14'W), Argentina

Salvador, J., Wolfram, E., Orte, F., Bulnes D., D'Elia, R., Quel, E.
CEILAP (CITEDEF-CONICET), UMI-IFAECI-CNRS 3351, Juan B. de La Salle 4397, B1603ALO Villa Martelli, Argentina.
Tel: +54-02966-15655090, E-mail: jsalvador@citedef.gob.ar
Zamorano, F., Casiccia, C.
Universidad de Magallanes (UMAG),
Punta Arenas, Chile

SUMMARY

The determination of temperature measurements from the Rayleigh scattering is an important remote sensing technique for obtaining stratospheric profiles. This technique is applied to signals acquired by a Rayleigh lidar (Light Detection and Ranging). Currently the Observatorio Atmosférico de la Patagonia Austral (51° 55'S, 69° 14'W) in Río Gallegos, Argentina is part of the UVO3Patagonia project in collaboration with the laboratory of Ozone and UV Radiation in the city of Punta Arenas, Chile distant 200 km, for more information www.uvo3patagonia.com. In this paper we showed the technique to measure temperature profiles in the stratosphere between 15-60 km altitude. We compared the temperature profiles obtained of the second ozone sounding campaign called OZITOS (**OZ**one profi**l**e a**T** Rí**O** Galleg**OS**) carried out in March 2011 in Río Gallegos with the temperature profile retrieved by the Rayleigh lidar using the line of 355 nm, in the same period. The results presented in this paper are validated through intercomparisons with measurements made by MLS instrument (Microwave Limb Sounder) onboard the NASA AURA satellite platform and NCEP data.

Key words: Rayleigh lidar, temperature profile, radiosounding measurements

INTRODUCTION

The lidar emerged as a powerful technique for the remote sensing of the atmosphere. The Rayleigh scattering due to air molecules has been widely used over the past 20 years to determine the temperature profile of the atmosphere between 30 and 90 km altitude. This method allows to study the dynamics of the middle atmosphere with high vertical resolution and temporal evolution. The extension of this technique to the lower atmosphere below 30 km is limited by aerosol scattering, ozone absorption, and dense atmospheric attenuation. To overcome these difficulties, the wavelength dependent non-elastic Raman scattering technique has been employed recently (Gross *et al.,* 1997) (Gu *et al.,* 1997) (Nedeljkovic *et al.,* 1993). However, Raman lidar requires a high-power laser transmitter to improve the low-level signal conditions because the Raman scattering cross section is about 3 orders of magnitude smaller than that of the Rayleigh scattering. Balloon borne instruments, rocket sounding, and satellite observations have been the main sources of information of this region. However, these datasets show many discrepancies and contain deficiencies due to poor vertical resolution and discontinuities. In this respect, the use of lidar, complements the other techniques, since the unique feature of lidar is its capability to make measurements of a number of important atmospheric parameters with excellent space and time resolution.
Since 2007, CEILAP group has installed the Observatorio Atmosférico de la Patagonia Austral. Actually we have a binational project with the laboratory of ozone and UV radiation ($LabO_3RUV$) from Magallanes's University called UVO3 Patagonia, supported by Japanese Cooperation Agency (JICA). Both groups are specialized in measured the depletion ozone using differents techniques. In CEILAP group basically can obtain ozone profile using a DIAL system described (Wolfram *et al.,* 2008). The $LabO_3RUV$ measured using ECC balloon sonde (Electrochemical Concentration Cell), developed by Komhyr (Komhyr 1969, 1971).
The final objective of this paper is to do an introduction to temperature profiles using a Rayleigh lidar which will be describe below. Also a campaign of ozonesounding made in Río Gallegos in March 2011, called OZITOS II (OZone profile aT RíO GallegOS) will be used to compare temperature profiles between 10 up to 32 km.
The analysis that we will make below is important to know since the campaign OZITOS II was principally designed for the validation of ozone profile. This paper try to use the temperature from radiosounding aboard the balloon sonde to compare the temperature profile obtained by the Rayleigh lidar temperature, and this way increase the capability of the instrument. Also we use the data from the National Centers for Environmental Prediction (NCEP) and the MLS instrument aboard satellite AURA-NASA (Acker and Leptoukh, 2007).

METHODOLOGY

The methodologies described in this section were separated in two parts: the first one describe how obtain a temperature profile from a Rayleigh lidar as a part of the DIAL system. The second one, tried describe the sensor used for the validation of temperature profile from Rayleigh lidar.

Rayleigh lidar temperature profiles

Lidar temperature measurements require that only molecular Rayleigh scattering contributes to the return signal and Mie scattering from aerosols is negligible. This is usually the case above 30 km, even after a volcanic eruption such as Mt. Pinatubo (Steinbrecht and Carswell, 1995). When the Mie scattering is not negligible which occurs typically below 30 km, the temperature value is lower than the real one due to the effects of aerosols.
The temperature algorithm only Rayleigh-scattered light signals produced by the atmosphere from the third harmonic of Nd-YAG laser at 355 nm were used. During the lidar measurements, the output of the multi-channel counters (MCS) provides the raw data as single ASCII files, with an integration time of 1 minute. The retrieval algorithm reads two raw data sets at 355 nm (high and low sensitivity), then performs a data integration variable from 1 to 3 hours. In the next step, two corrections are applied to remove systematic errors in the signals: background signals, Signal-Induced Noise (SIN). The objective of these corrections is to obtain a pure lidar backscattering signal. Then both corrected signals are merged by means of linear fitting in the 20-25 km range.
After this corrections, we retrieved the temperature profile from the lidar signal.

ECC sondes

The balloon sondes used during OZITOS II campaign are configured by a radiosounding and an ECC which is the responsible for the detection of ozone concentration. In our experiment the ECC sonde launched has also a radiosounding which can measure temperature, humidity and pressure.
The radio receptor is a Lockheed Martin LMG6. It was used for store all data emitted by the sonde. As sensor we used a meteorological radiosounding LMS6. An ECC model EN-SCI Corporation was used for measure the ozone concentration.

OZITOS II CAMPAIGN

In December 2008, the instrument DIAL for the measurements of stratospheric ozone profile deployed in the Patagonian city of Río Gallegos was accepted as part NDACC (Network for the Detection Atmospheric Composition Change). This new stage of the instrument must satisfy new requirements as intercomparisons with other kind of sensor to check the stability and guarantee a quality in the measurements. Very often different groups around the world used ECC balloon sondes for measured ozone concentration in a region between the surface up to 30 km aprox.
Though the principal objective was to make validations between DIAL and ECC balloon sondes, this paper showed the comparison between temperature profile derived with the 355 nm line as described above and the temperature profile measured with the radiosounding, during OZITOS II campaign.

Experimental design

The night March 17, 2011 both groups decided to lunch in a same night three balloon sonde in coincidence with the DIAL operation. The aim was study the minimum time of integration in the data files acquired by DIAL systems. The schedule of the experimental design is showed in Figure 1.

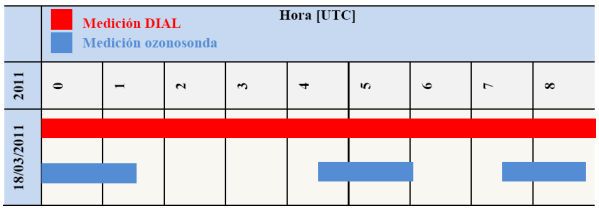

Figure 1. Schedule of measurement made in the OAPA during OZITOS II campaign in March 17, 2011. The red bar is the time that the lidar were measuring and blue bar the period of flight of each ozonesounding.

Where the horizontal red bar indicate the total time of measurement of the DIAL system and the blue bar indicate the time of flight of the ozonesounding. Can you show that the DIAL systems was operating more than nine hours. If we select a time of integration of three hours we can obtain three independent measurements that each one can be compared with each balloon sonde launched (same period time of flight). Now we can decrease the time of integration, and we can derivate for example more profiles.
The advantage using signals obtained by a DIAL system, is that we can use the signals in 355 nm from the Nd:YAG laser for retrieved a temperature profile without produced any interference on the ozone measurements.

Results and discussion

We have taken from the total measurement about nine hours from Rayleigh, three independent period of time which we calculated the temperature profile using a time of 180 minutes of integration. This time is quasi-coincident with the time of flight of the ozonesounding launched beside, 1 km away of the DIAL system in Río Gallegos. This means that we can compare temperature derived from both instruments.
In Figure 2, we showed the comparison of the temperature profile between the Rayleigh lidar temperature and the radiosounding.

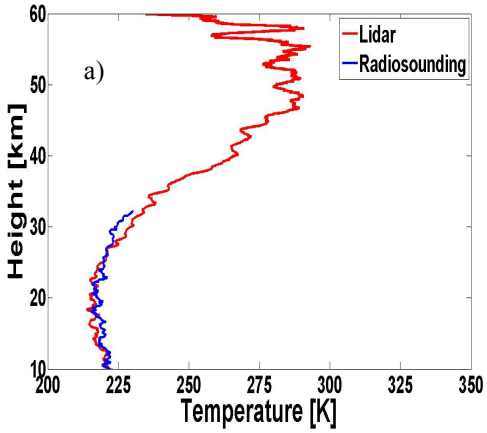

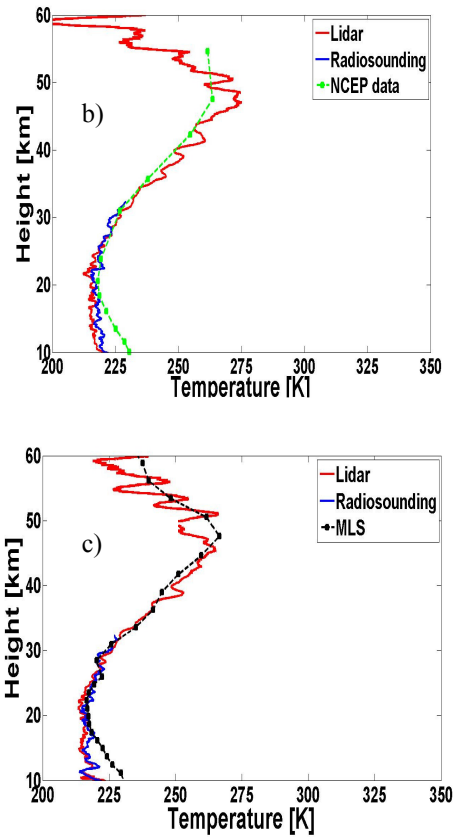

Figure 2. Comparison of the temperature profiles; a), b), c) are the temperature profile by the Rayleigh lidar (red line) compared with radiosounding (blue line). b) show the comparison with NCEP data (dashed green line with square) for March 17, 2011 in Río Gallegos and c) show the comparison with a MLS sensor(dashed black line with square) aboard AURA-NASA in March 17, 2011 lat=-51.74 °, lon= -75.23 °, time: 06:03:09 (UTC).

The region of comparison between both instruments is a disvantage due they have different heights of cover.
In the case of the Rayleigh lidar we can obtain temperature profile from aprox. 10 km up to 60 km. While in the balloon sonde only we can measured temperature profile between the surface up to 32 km. The effective zone where both instruments can be compared, cover the range 10 to 32 km, aprox, limited in the lower part for the lidar and in the higher part for the balloon burst altitude.
The Figure 2 has shown the good agreement between the diferent profiles, having a relative error lidar - radiosounding lower than 4 %. Additional in b) we superposed the NCEP data for the same day of measurement, and c) show the comparison with the data provided by the MLS instrument aboard the plataform AURA-NASA.

CONCLUSION

This paper has shown three independent temperature profiles derivated with a Rayleigh temperature lidar for one day (March 17, 2011). These profiles were obtained as a part of the OZITOS II Campaign described above. In each measurement the Rayleigh temperature profiles were compared with the radiosounding aboard the balloon sonde. The effective region for the comparison can be established due figure 2 in the region between 10 up to 30 km aprox. Both instruments have shown good agreement in this region, with a typical relative error lower than 4 %. We have observed also that in this night the three lidar profiles are similar, indicating that the atmospheric conditions were stable. As a comparison with other instrument as the NCEP data and MLS instrument aboard the AURA-NASA satellite has been to do it. It measurements were superposed in the profiles b) and c) (figure 2) showing very good agreement in the region above 20 km. For the region below both measurements (NCEP data and MLS) indicate a discrepancy very similar when are compared with the radiosounding and temperature lidar profiles.

ACKNOWLEDGMENTS

The authors would like to thank JICA (Japan International Cooperation Agency) by financial support of UVO_3 Patagonia Project; the CNRS in France for their collaboration in facilitating the shelter and part of the electronic instruments of DIAL.
Analyses used in this paper were produced with the Giovanni online data system, developed and maintained by the NASA GES DISC.

REFERENCES

Acker and, J. G., G. Leptoukh, (2007), Online Analysis Enhances Use of NASA Earth Science Data", Eos, Trans. AGU, Vol. 88, No. 2, pages 14 and 17.

Gross, M.R., McGee, T.J., Ferrare, R.A., Singh, U.N., Kimvilakani, P, (1997), Temperature measurements made with a combined Rayleigh–Mie and Raman lidar, Applied Optics ,36, pp, 5987–5995.

Gu, Y.Y., Gardner, C.S., Castleberg, P.A., Papen, G.C., Kelley, M.C, (1997), Validation of the lidar in-space technology experiment: stratosphere temperature and aerosol measurements,Applied Optics, 36, pp, 5148–5157.

Komhyr, W.D., (1969), Electrochemical concentration cells for gas analysis, *Ann. Geoph., 25,* 203-210.

Komhyr, W.D., (1971), Development of an ECC-Ozonesonde, *NOAA Techn. Rep. ERL 200-APCL 18ARL-149.*

Nedeljkovic, D., Hauchecorne, A., Chanin, M.L, (1993), Rotational Raman lidar to measure the atmospheric-temperature from the ground to 30 km, IEEE Transactions on Geoscience and Remote Sensing, 31,pp, 90–101.

Steinbrecht, W., and A.I. Carswell, (1995), Evaluation of the effect of Mount Pinatubo aerosol on differential absortion lidar measurements of stratospheric ozone. J.Geophys. Res.100, 1215-1233.

Wolfram, A. E., J. Salvador, R. D'Elia, C. Casiccia, N. Paes Leme, A. Pazmiño, J. Porteneuve, S. Godin-Beekman, H. Nakane and E. J. Quel, (2008), New Differential absorption lidar for stratospheric ozone monitoring in Patagonia, south Argentina, J. Opt. A: Pure Appl. Opt. 10, 104021 (7pp). oi:10.1088/1464-4258/10/10/104021.

REVISTA BOLIVIANA DE FÍSICA 20s, 36-38, 2011
ISSN 1562-3823. INDEXADA EN: SCIELO, LATINDEX, PERIÓDICA

Optical study of the laser beam propagation on Nd:YAG crystal slab for space LIDAR missions

Kosmas Gazeas, George Tzeremes and Errico Armandillo
European Space Agency, ESTEC, Mechatronics and Optics Division
Keplerlaan 1, 2200AG, Noordwijk, The Netherlands
Tel: +31 71 5656743, Fax: +31 71 5655430, E-mail: Kosmas.Gazeas@esa.int, kgaze@physics.auth.gr

SUMMARY

The present paper reports on the development of a simulation and modeling tool which allows to estimate the propagation effects on a laser beam passing through a laser-diode-pumped Nd:YAG slab amplifier. This in-house research work is motivated by current ESA spaceborne LIDAR programs (ADM, Earth Care) as a mean to provide understanding of the LIDAR beam pointing stability as results of thermal and mechanical stresses. A dynamic model has been generated that can simulate the optical characteristics of the laser beam propagation, as a result of the various thermal and mechanical processes occurring inside the laser Pumping Unit and the thermal lensing occurring along the crystal slab. The simulation results and their comparison with actual laboratory tests are being presented and discussed. The model developed is based on the Finite Element Model (FEM) methodology, where the slab as an active element is "broken" down into interdependent segments, each simulated as being heated by an individual LD source. The light beam is propagated along the slab using dynamically varying boundary conditions, to the next so to account for the cumulated thermal and mechanical loads.

Key words: Nd:YAG laser, thermal lensing, LIDARS

INTRODUCTION

LIDARs in space require reliable operation of high power laser transmitters. It is the case for ESA ADM and EarthCare missions where high power UV lasers are being used in an oscillator-multipass amplifier configuration to reach the required energy level and characteristics (Figure 1). ESA space LIDAR programs use both high power Nd:YAG slab, with diode-laser (LD) pumped. In these configurations, thermo-mechanical behavior of the slab can affect seriously the output laser beam characteristics, specifically the most critical variables which can play an important role in the output laser beam are the:

- Coldplate temperature (TCP)
- Laser Diode physical characteristics and location
- Slab geometry
- Input beam characteristics
- Collimating optics
- Operating conditions (air/vacuum, ambient temp.)

To model such processes, it is to be noted that since the number of variables is too large to allow a closed form solution for the thermal lensing of the crystal slab, Finite Element Method (FEM) is proposed and used to compute the combined thermal, mechanical and optical effects.

MOTIVATION OF THIS WORK

The final goal is to achieve fully controlled boundary conditions and direct view of the outgoing laser beam. This way we can predict the necessary modifications needed to preserve the laser energy and amplification efficiency reducing energy loss at minimum. Also we will have the ability to predict the outgoing laser beam profile and divergence. This will give direct information for the actual lenses need to be applied before and after the PU, in order to focus the beam and preserve its shape and energy density.

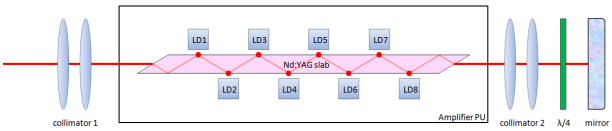

Figure 1. A schematic of the amplifier PU.

Nd:YAG CRYSTAL SLAB GEOMETRY

The crystal slab geometry is shown in Figure 2. A laser beam with a Gaussian profile at 1064 nm enters the crystal parallel along the long axis and bounces 5 times on the top and 5 on the bottom inner surfaces. The other two side surfaces are attached to the cold plates, pumping out the accumulated heat. Boundary conditions are controlled by heat drain from the two cold plates and the energy emitted from the 8 pumping laser diodes at 808 nm.

THERMAL LENSING

Thermal lensing effects take place along the crystal slab, as the thermal profile is variable. As a consequence, the refractive index is variable, following the thermal profile, as described by Shellmeier equations. For every finite cross section of the slab, a thermal profile is calculated, following boundary